





20 **Abstract:** The lightning assimilation (LTA) technique in the Kain-Fritsch convective  
21 parameterization in the WRF model has been updated and applied to continental and hemispheric  
22 simulations using lightning flash data obtained from the National Lightning Detection Network  
23 (NLDN) and the World Wide Lightning Location Network (WWLLN), respectively. The impact  
24 of different values for cumulus parameters associated with the Kain-Fritsch scheme on  
25 simulations with and without LTA were evaluated for both the continental and the hemispheric  
26 simulations. Comparisons to gauge-based rainfall products and near-surface meteorological  
27 observations indicated that the LTA improved the model's performance for most variables. The  
28 simulated precipitation with LTA using WWLLN lightning flashes in the hemispheric  
29 applications was significantly improved over the simulations without LTA when compared to  
30 precipitation from satellite observations in the Equatorial regions. The simulations without LTA  
31 showed significant sensitivity to the cumulus parameters (i.e., user-toggled switches) for monthly  
32 precipitation that was as large as 40% during convective seasons for month-mean daily  
33 precipitations. With LTA, the differences in simulated precipitation due to the different cumulus  
34 parameters were minimized. The horizontal grid spacing of the modeling domain strongly  
35 influenced the LTA technique and the predicted total precipitation, especially in the coarser  
36 scales used for the hemispheric simulation. The user-definable cumulus parameters and domain  
37 resolution manifested the complexity of convective process modeling both with and without  
38 LTA. These results revealed sensitivities to domain resolution, geographic heterogeneity, and the  
39 source and quality of the lightning dataset.

## 40 **1. Introduction**

41       Thunderstorms are natural phenomena that have intrigued human imagination for  
42 thousands of years. Although early efforts in atmospheric science and modeling were focused on



43 understanding and forecasting thunderstorms, they remain difficult to accurately simulate in  
44 meteorological models. A variety of lightning parameterization schemes have developed in  
45 regional and global atmospheric models (Price and Rind, 1992; Romps et al., 2014; Finney,  
46 2014; Lopez, 2016) based on various physical, dynamical, and cloud properties, but these  
47 schemes marginally reproduce the spatial and temporal variability of lightning flashes with  
48 varying success over different regions of the globe. With the advancement of lightning detection  
49 technologies both at ground level and via satellite in the past decades, observed lightning flashes  
50 with coverage from regional to global scales are available and can be used for lightning  
51 assimilation (LTA). A robust LTA can improve convective simulations in meteorological models  
52 for retrospective atmospheric simulations (e.g., Heath et al., 2016; Marchand and Fuelberg,  
53 2015) or help generate better initial fields for real-time weather forecasting (e.g., Lagouvardos et  
54 al., 2013; Giannaros et al., 2016; Fierro et al., 2012, 2015) by pinpointing where deep convection  
55 occurred and altering the meteorology in what is generally referred to as a hot start (Gan et al.,  
56 2021).

57 Heath et al. (2016) implemented an LTA technique in the Kain-Fritsch (KF) convective  
58 scheme in the Weather Research and Forecasting (WRF) model using lightning observations  
59 from the National Lightning Detection Network (NLDN) over the contiguous United States  
60 (CONUS). They found that the simulation of warm-season rainfall was substantially improved,  
61 and other near-surface meteorological variables were clearly improved in retrospective WRF  
62 applications. Lightning also profoundly impacts the chemical composition of the troposphere by  
63 generating and releasing nitrogen oxides ( $\text{LNO}_x$ ) that can significantly alter ground-level ozone  
64 ( $\text{O}_3$ ) concentrations in some regions (Kang et al., 2020). Because meteorological models drive air  
65 quality simulations, improving meteorological variables with LTA will cascade to chemistry



66 fields simulated by air quality models. It is especially critical when LNO<sub>x</sub> emissions are included  
67 in air quality models, since LTA is designed to align LNO<sub>x</sub> emissions with the time and location  
68 when atmospheric convection occurred in the model, so the subsequent chemistry reactions and  
69 transport will more accurately reflect the emissions from lightning (Kang et al., 2019a and  
70 2019b).

71 Heath et al. (2016) implemented the LTA technique in WRFv3.8 and tested for several  
72 month simulations. The LTA technique has been implemented in subsequent WRF releases (not  
73 publicly available yet) and applied in many meteorology and air quality studies over the CONUS  
74 (e.g. U.S. EPA, 2019; Appel et al, 2021). Although using LTA improved the predicted  
75 meteorological variables, some occasional unwanted departures from base model predictions  
76 without LTA occurred. Most commonly, LTA resulted in a low bias in summertime rainfall in  
77 some regions (U.S. EPA, 2019).

78 For this reason, it is of interest to investigate two parameters associated with the KF  
79 convective scheme with different optional values, which are specified in the WRF runtime  
80 namelist input file, are often encountered by WRF users  
81 ([https://www2.mmm.ucar.edu/wrf/users/docs/user\\_guide\\_v4/contents.html](https://www2.mmm.ucar.edu/wrf/users/docs/user_guide_v4/contents.html)). One parameter is  
82 called kfeta\_trigger (also referred to as trigger for simplicity in this paper) which controls the  
83 conditions to determine how the KF convective scheme is triggered with three optional values: 1,  
84 the default value; 2, moisture-advection based trigger (only for ARW - the advanced research  
85 WRF dynamical solver); and 3, RH-dependent additional perturbation to Option 1 (not tested).  
86 Another parameter is called cudt (namely **c**umulus time interval, **d**elta **t**) and its value determines  
87 the minutes between cumulus physics calls (here it is the KF scheme). The default value of 0  
88 indicates that the cumulus physics is called at every model step, and any non-zero value specifies



89 the interval (minutes) that the cumulus physics is called (for example,  $cudt=10$  means that the  
90 cumulus physics is called every 10 minutes). Even though some discussions and  
91 recommendations regarding the choice of these parameter values through online forums or WRF  
92 user mailing list (e.g., <https://forum.mmm.ucar.edu/>; <https://wrfems.info/>;  
93 [https://www.epa.gov/sites/default/files/2017-02/documents/wrf\\_with\\_ltga\\_userguide.pdf](https://www.epa.gov/sites/default/files/2017-02/documents/wrf_with_ltga_userguide.pdf)), but no  
94 literature evaluates how these parameter values impact model performance when LTA is used.

95 Heath et al. (2016) demonstrated that the LTA technique consistently improved the  
96 simulation of precipitation and other near surface variables, but the evaluation was limited to the  
97 CONUS, reflecting the areal coverage of NLDN (Murphy et al., 2021). As the spatial  
98 applications of atmospheric composition modeling are expanded from regional to hemispheric  
99 and global scales and new lightning datasets are available, there is a strong need to examine how  
100 this LTA technique performs at these larger scales when lightning flash data from a less accurate  
101 detection network are used. Thus, lightning flashes from the World Wide Lightning Location  
102 Network (WWLLN, operated by the University of Washington: <http://www.wlln.com>) is a  
103 suitable candidate because it has the global coverage with affordable cost, albeit its detection  
104 efficiency is lower than the  $>95\%$  of NLDN (Abarca et al., 2010).

105 Our research has multiple objectives based on the aforementioned open research needs:  
106 1) assess the impact of the parameter values associated with the KF convective scheme on WRF  
107 performance over the CONUS domain without LTA (BASE case) and with LTA using lightning  
108 flashes from NLDN; 2) examine the LTA in WRF using lightning flashes from WWLLN and  
109 compare to the simulations with NLDN lightning flashes; and 3) apply LTA to WRF simulations  
110 over the Northern Hemisphere and evaluate the performance in terms of precipitation and near-  
111 surface meteorological variables. In section 2, we describe the updates made to the initial LTA



112 technique (Heath et al., 2016). Section 3 provides the detailed data and methodologies of the  
113 model simulations and their evaluation. Section 4 presents our analysis on the impact of  
114 parameters with KF convective schemes with and without lightning assimilation over CONUS  
115 using lightning flashes from NLDN and WWLLN. In section 5, we analyze the use of lightning  
116 flashes from WWLLN for LTA and evaluate WRF simulations with and without LTA over the  
117 Northern Hemisphere. And we conclude with key findings and recommendations in section 6.

## 118 **2. Updates on the LTA technique**

119         The lightning assimilation used here is based on Heath et al. (2016), which extended the  
120 works of Rogers et al. (2000), Mansell et al. (2007), Lagouvardos et al. (2013), and Giannaros et  
121 al. (2016). In general, the lightning assimilation approach used here is straightforward,  
122 activating deep convection where lightning is observed and only allowing shallow convection  
123 where it is not. This method is applied in the Kain-Fritsch scheme in WRF (Kain, 2004). A full  
124 description of the method can be found in Heath et al. (2016). Here, we provide only the  
125 essential details, along with recent modifications to the scheme.

126         First, the lightning data (WWLLN or NLDN) is binned to the WRF domain in both time  
127 and space. The temporal binning is done every 30 min and includes lightning data from -10 min  
128 to +20 min of the current time. The spatial regridding searches for a lightning strike within each  
129 grid box (using the staggered grid edge coordinates) within each time bin. This process creates a  
130 new lightning file with the same horizontal dimensions as the WRF domain filled with zeros (no  
131 lightning) or ones (lightning) at each 30-minute time step. During the WRF simulation, if  
132 lightning is present, the scheme first goes through its standard updraft calculations, except that it  
133 uses the layer with the greatest moist static energy as its updraft source layer (USL). If the  
134 resulting cloud does not meet the criteria for deep convection, 0.1 g kg<sup>-1</sup> of water vapor and 0.1



135 K are incrementally added to the USL until deep convection is forced. In the original Heath et  
136 al. scheme, only moisture was added to the USL. We have included temperature perturbations to  
137 further promote activating deep convection in these grid points with lightning.

138 In the unmodified KF scheme, a cloud must exceed a minimum depth (as a function of  
139 cloud base temperature) to satisfy the deep convection criteria. Heath et al. (2016) modified this  
140 depth for lightning assimilation to be more consistent with lightning-producing storms.  
141 Specifically, within WRF, storms with a base temperature greater than or equal to 20°C must  
142 have a cloud depth of at least 6 km with a cloud top temperature less than -20°C. Similarly, in  
143 the original model in Heath et al., storms with a cloud base temperature less than 20°C must have  
144 a cloud depth of at least 4 km and a cloud top temperature less than -20°C. These criteria were  
145 set to ensure that sub-grid deep convective clouds were deep enough to have a mixed-phase layer  
146 to support lightning (e.g., Mansell et al., 2007; Bruning et al., 2014; Preston and Fuelberg, 2015).  
147 In this study, we slightly modified the scheme to require that the cloud top is at least one model  
148 level above the -20°C level, ensuring cloud-top temperatures are less than -20°C (e.g.,  
149 Stolzenburg and Marshall, 2009). The prior limit at -20°C could inadvertently weaken simulated  
150 deep convective clouds, which may contribute to the dry bias in earlier applications of lightning  
151 assimilation approaches (U.S. EPA, 2019).

152 In Heath et al. (2016), if deep convection could not be achieved after incrementally  
153 adding up to 1 g kg<sup>-1</sup> to the USL (which is now 1 g kg<sup>-1</sup> and 1 K in our update), then no further  
154 action was taken, and deep convection was not activated by KF. However, to increase the  
155 realism of the scheme and increase the odds of deep convection the next time the scheme is  
156 called, we have updated the approach as follows. If a deep convective cloud cannot be activated,  
157 the tallest cloud created is passed into the KF shallow convection scheme. In the KF scheme,



158 shallow clouds are re-diagnosed each time the scheme is called. For example, suppose a shallow  
159 cloud is generated at  $t=0$  and KF is called at 5 min intervals. In that case, at the  $t=5$  min call, KF  
160 would determine if a shallow cloud is still present. Thus, the cloud can evolve so that at  $t=5$  min  
161 it could have slightly different characteristics than the one diagnosed at  $t=0$ . This allows shallow  
162 clouds to grow, decay, or persist at short timescales.

163 Therefore, if the LTA method cannot trigger deep convection, the shallow cloud that is  
164 generated within WRF can precondition the atmosphere, thus increasing the likelihood of deep  
165 convection the next time the KF scheme with LTA is called. Therefore, these refinements to the  
166 LTA scheme in KF more closely replicate how convective initiation is observed in nature, where  
167 shallow cumulus and congestus clouds precondition the environment prior to deep convection  
168 initiation.

169 Lastly, at grid points without observed lightning, deep convection is suppressed in WRF,  
170 and only the shallow portion of KF is allowed to run. Because convective clouds in nature can  
171 form and precipitate without generating lightning, this suppression technique serves as a realistic  
172 approach to reproduce nature given the constraints of the KF parameterization.

173

### 174 **3. Data and Methodology**

#### 175 3.1. Lightning flash data

176 Lightning flash data from two ground-based lightning detection networks were used for the  
177 assimilation using the LTA technique in this study. The NLDN provides cloud-to-ground  
178 lightning observations with a detection efficiency of  $>95\%$  and a location accuracy of about 150  
179 m (Murphy et al., 2021) over the contiguous U.S. (CONUS). The WWLLN provides global



180 lightning data with lower detection efficiency and location accuracy (Abarca et al., 2010;  
181 Rudlosky and Shea, 2013; Burgesser, 2017) compared to NLDN and the Lightning Imaging  
182 Sensor (LIS) observations (Mach et al., 2007). Since WWLLN has global coverage, even with its  
183 relatively lower detection efficiency and location accuracy compared to NLDN, it could be a  
184 good option for applications beyond CONUS. Figure 1 shows how the average lightning flash  
185 rate (flashes  $\text{km}^{-2}\text{hr}^{-1}$ ) from WWLLN compares to NLDN during July and September 2016 when  
186 hourly lightning flash counts are gridded into the CONUS 12-km grid cells.

187 As shown in Figure 1, the lightning flash rates in NLDN are much higher than those in  
188 WWLLN, especially during July and over the land, and this is generally true (not shown) that  
189 NLDN reported more lightning flashes than WWLLN during warm months over land. The  
190 differences are much smaller during cool months and over the coastal regions where NLDN has  
191 coverage. Note that the absolute difference in flash count may not necessarily translate  
192 proportionally into convective activities in terms of LTA because the LTA technique as  
193 described in Heath et al. (2016) depends on the detection of lightning occurrence (binary “yes”  
194 or “no” situation), not the actual flash count, in a specific time interval at a grid cell.

### 195 3.2. Precipitation Data

196 The daily precipitation from the Parameter-elevation Regressions on Independent Slopes  
197 Model (PRISM)’s high-resolution spatial climate data for the United States  
198 ([https://climatedataguide.ucar.edu/climate-data/prism-high-resolution-spatial-climate-data-](https://climatedataguide.ucar.edu/climate-data/prism-high-resolution-spatial-climate-data-united-states-maxmin-temp-dewpoint)  
199 [united-states-maxmin-temp-dewpoint](https://climatedataguide.ucar.edu/climate-data/prism-high-resolution-spatial-climate-data-united-states-maxmin-temp-dewpoint)) is used to evaluate WRF-simulated precipitation over the  
200 CONUS, and the NOAA Climate Prediction Center (CPC)’s global unified gauge-based analysis  
201 of daily precipitation (<https://psl.noaa.gov/data/gridded/data.cpc.globalprecip.html>) product is  
202 employed to assess WRF’s hemispheric precipitation predictions. The daily total PRISM



203 precipitation data are available at 4-km horizontal grid spacing over the CONUS, and the annual  
204 CPC precipitation (partitioned into daily totals) is available globally at  $0.5^\circ$  latitude  $\times$   $0.5^\circ$   
205 longitude grid ( $720 \times 360$ ) resolution. These datasets were regridded to the WRF modeling  
206 domains for the 12-km CONUS and the 108-km Northern Hemisphere to pair with model  
207 simulations in time and space. To assess the simulated precipitation over the oceans, especially  
208 in the tropical regions where no gauge-based measurement is available, products from the Global  
209 Precipitation Measurement (GPM) (Huffman et al., 2015; Asong et al., 2017), a joint mission co-  
210 led by NASA and the Japan Aerospace Exploration Agency (JAXA) and comprised of an  
211 international network of satellites that provide the next-generation global observations of rain  
212 and snow, are employed. The Integrated Multi-satellitE Retrievals for GPM (IMERG) Long-term  
213 Precipitation Data Products  
214 (<https://arthurhouhttps.pps.eosdis.nasa.gov/gpmdata/YYYY/MM/DD/imerg/>; registration is  
215 required for access) cover the entire globe with  $0.1^\circ$  latitude  $\times$   $0.1^\circ$  longitude grid resolution. To  
216 compare with WRF simulated hemispheric precipitation, the daily mean precipitation data from  
217 the IMERG V06 dataset from 2016 is regridded onto the hemispheric WRF domain  
218 (<https://gpm.nasa.gov/data/directory>). The research-quality gridded IMERG V06 dataset Final  
219 Run product estimates precipitation using quasi-Lagrangian time interpolation, gauge data, and  
220 climatological adjustment.

### 221 3.3. Ground-Based Meteorological Data

222 The impacts of user-definable parameter values associated with KF and datasets for LTA  
223 were quantified for simulated near-surface meteorological variables such as precipitation, 2-m  
224 temperature (T2), water vapor mixing ratio, wind speed and wind direction. The simulated  
225 meteorological fields from WRF are compared against observations from NOAA National



226 Centers for Environmental Information (NCEI) land-based stations, which are archived from  
227 data collected globally (<https://www.ncei.noaa.gov/products/land-based-station>). The  
228 Atmospheric Model Evaluation Tool (AMET) (Appel et al., 2011) is used to pair surface  
229 observations with model predicted values in both space (bilinear interpolation) and time (hourly).

### 230 3.4. Model Configurations and Simulation Details

231 The WRF model (Skamarock and Klemp, 2008) version 4.1.1 (WRFv411,  
232 <https://github.com/wrf-model/WRF/releases/tag/v4.1>) with LTA updates to Heath et al. (2016)  
233 (as described in Section 2) is used to perform simulations over the CONUS and the hemispheric  
234 domains. The CONUS domain is configured with 36 vertical levels and 12-km horizontal grid  
235 spacing with  $472 \times 312$  grid points. The hemispheric domain is configured with 45 vertical  
236 levels and 108-km horizontal grid spacing with  $200 \times 200$  grid points that covers the entire  
237 Northern Hemisphere and the northern border of the Southern Hemisphere along the Equator.  
238 The simulation period for CONUS simulations is from April–July in 2016 with 10-day spin-up  
239 period from March 22; for the hemispheric domain, annual simulations for 2016 are performed.  
240 Our analysis focuses on July when convective activities are often the most prevalent over the  
241 CONUS; other months are examined in the hemispheric simulations which simulate the year-  
242 round convective activities in the tropics. The detailed configurations of cloud microphysics,  
243 land surface parameters, radiation schemes, and four-dimensional data assimilation (FDDA) are  
244 the same as described in Heath et al. (2016) and sample WRF namelist input files for both the  
245 CONUS and hemispheric simulations are included in the supplementary information (Table S1  
246 and Table S2).

247 The KF scheme includes two options to trigger convective activity. Trigger 1 is based on  
248 a mass-conservative cloud model, which includes parameterized moist downdrafts, entrainment,



249 and detrainment at the cloud edge (Kain and Fritsch, 1990, 1993) and allows interaction between  
250 cloud and environment, and it is the default option for most applications. Trigger 2 is an alternate  
251 option based on Ma and Tan (2009), and that is a moisture-advection modulated trigger function  
252 to improve results in subtropical regions when large-scale forcing is weak. In addition, the KF  
253 scheme is called by default at every time step, but it can be configured to only update convective  
254 parameters on a user-definable time increment. In this study, sensitivities are conducted to the  
255 version of the KF trigger (i.e., Trig1 and Trig2, abbreviated as K1 and K2 in Table 1,  
256 respectively), as well as to frequency at which KF is called (i.e., “cudt”). Two sensitivities on  
257 cudt were performed: one where KF is called at each model integration time step (i.e., “Cudt0”,  
258 abbreviated as C0 in Table 1), and the other where KF is updated every 10 minutes of integration  
259 time (i.e., “Cudt10”, abbreviated as C10 in Table 1). The sensitivities to KF trigger and update  
260 frequency are combined in a matrix of simulations that also are conducted with/without LTA,  
261 and they are listed in Table 1. All eight simulations are performed for both the CONUS and the  
262 hemispheric domains. For LTA cases, lightning flashes from both NLDN and WWLLN are used  
263 over the CONUS domain and lightning flashes from WWLLN are used for the hemispheric  
264 domain. For convenience of description, the cases without LTA are collectively referred to as  
265 BASE cases, and the cases with LTA are referred to as LTA cases. To further distinguish the  
266 lightning networks, the LTA cases are also referred to as LTA NLDN (or simply NLDN) and  
267 LTA WWLLN (or simply WWLLN) cases, respectively.

### 268 3.5. Evaluation Methodologies

269 The assessment of the impact of LTA on model performance is focused on precipitation  
270 since that is the most affected variable, though other near-surface variables are also evaluated.  
271 Due to the highly heterogeneous nature of thunderstorms and lightning over space, in addition to



272 examining the overall statistics across the modeling domain, statistics are analyzed to assess the  
273 impact of LTA over U.S. climate regions ([https://www.ncei.noaa.gov/monitoring-  
275 references/maps/us-climate-regions](https://www.ncei.noaa.gov/monitoring-<br/>274 references/maps/us-climate-regions)) in both domains and some of the larger countries in the  
276 hemispheric simulations. Figure 2 shows these climate regions over the CONUS modeling  
277 domain and the selected countries (also referred to as regions) in the hemispheric modeling  
278 domain.

278 The statistical metrics in this analysis include the widely used correlation coefficient ( $r$ )  
279 to measure the linear association of measured and simulated variables, mean bias (MB) and  
280 normalized mean bias (NMB) to quantify the departure of simulated values from measured  
281 values, and root mean square error (RMSE) and normalized mean error (NME) to elucidate the  
282 errors associated with model simulations. More emphasis is placed on certain metrics than others  
283 depending on the nature of the simulated quantity. For instance, with precipitation, correlation  
284 coefficient (if the model can simulate rainfall at the right time and location) and MB and NMB  
285 (if the model over- or under-estimate rainfall amount) are more straightforward than the error  
286 metrics (though they are still relevant), but MB and NMB are inappropriate to evaluate wind  
287 directions.

288

#### 289 **4. CONUS WRF Simulations**

290 As shown in Table 1, four BASE (without LTA) cases, four LTA cases using lightning flash  
291 data from NLDN, and four LTA cases using lightning flash data from WWLLN over the  
292 CONUS domain were performed using the combinations of two trigger options and two  
293 convective update (cudt) intervals, respectively. For the LTA cases, when lightning flashes were  
294 not present, the ShallowOnly option (Heath et al., 2016) was used (Table S1).



295 4.1. Precipitation

296 Figure 3 displays the July 2016 mean statistics generated by pairing the gridded WRF  
297 precipitation with the values from PRISM in time and space for each of the U.S. climatological  
298 regions. As shown in Figure 3, the BASE simulations present the most dramatic fluctuations  
299 among cumulus parameter sensitivities than the LTA cases. With Trig1, when the cutd is  
300 changed from 0 to 10, the correlation coefficient is substantially reduced across all the regions  
301 (Figure 3a), and increases in biases (overestimate of precipitation, Figures 3b&c) and errors  
302 (Figures 3d&e) are also worsened by less frequent cumulus updates. With trigger 2, the biases  
303 (MB and NMB) changed from overestimation to underestimation, and the errors (RMSE and  
304 NME) were smaller compared to Trig1. Though the setting for cutd altered simulations with  
305 Trig2, the difference was smaller than the cases with Trig1. In general, the Trig1 cases tended to  
306 produce more precipitation (overestimate compared to PRISM precipitation) than the Trig2 cases  
307 (underestimate compared to PRISM precipitation), and the Cudt10 cases generated more  
308 precipitation than the Cudt0 cases. Among the four cases in the BASE model simulations, the  
309 K1C0 case (Trig1, Cudt0) is the most favorable in terms of the correlation coefficients and  
310 precipitation biases, but the error statistics, especially NME, may not be the most desirable.

311 Using LTA (Figure 3), the correlation coefficients significantly increased over the  
312 domain and across the regions (from the range of  $\sim 0.25$  to  $\sim 0.40$  to the range of  $\sim 0.30$  to  $\sim 0.48$ )  
313 relative to the BASE cases. Though the LTA WWLLN cases had lower correlation compared to  
314 the LTA NLDN cases due to the lower detection efficiency of lightning flashes in WWLLN, the  
315 improvement was still rather considerable compared to the BASE cases. The biases in the LTA  
316 NLDN cases are most favorable with values negative but closest to zero (small underestimate).  
317 The LTA WWLLN cases produced larger negative biases than the BASE cases and LTA NLDN



318 cases, again, related to detection efficiency of the networks. All the LTA cases (both NLDN and  
319 WWLLN) produced smaller errors than the BASE cases, and the differences between the NLDN  
320 cases and WWLLN cases were minimal. Comparing the LTA cases with the BASE cases, one  
321 noticeable feature is that with the different trigger and cutd values, all the statistics fluctuated  
322 dramatically from one case to another in the BASE cases, but fluctuation among the LTA cases  
323 was minimized and negligible. This is expected, as the moisture and temperature perturbations  
324 used to trigger convection with LTA (Section 2) will take precedence over the trigger options  
325 and grouping the lightning data into 30-minute bins should mitigate the influence of the cutd  
326 option. These features were deliberately incorporated into the LTA technique for precisely these  
327 reasons, but this paper documents their systematic testing.

328       Examination of the statistics across the climatological regions over the CONUS domain  
329 indicates that the Ohio Valley (OVC) stands out among all the regions with the lowest  
330 correlation coefficients and largest RMSE values in all the BASE cases. However, with LTA, the  
331 correlation coefficients in OVC were brought to the median range among other regions, though  
332 the RMSE values were still the largest in that region; these features in OVC are more  
333 understandable as manifested in Figure 12, examined in detail in Section 5. Other statistics in  
334 OVC with LTA were comparable with other regions except for relatively larger negative MB  
335 values associated with the LTA WWLLN cases. Another obvious characteristic with regards to  
336 correlation coefficients and errors (RMSE and NME) was that there was more spread among the  
337 regions in the LTA cases than in the BASE cases (except in OVC), which resulted from the  
338 geographically heterogeneous nature of convective precipitation and the associated observed  
339 lightning intensity across the regions.



340 To alleviate the underestimation of precipitation in the LTA WWLLN cases, additional  
341 simulations (K1C10Ws0 and K2C10Ws0; where K1C10W and K2C10W are the same as in  
342 Table 1, while s0 means zero suppress when lightning flash is not present) were performed by  
343 switching the suppression option as described in Heath et al. (2016) from “ShallowOnly” to  
344 “NoSuppress.” This modification still triggers deep convection where lightning is observed;  
345 however, at grid points without lightning, the KF scheme is configured to run normally (i.e., the  
346 same as in the BASE cases). As shown in Figure S1, the correlation coefficients in the  
347 WWLLN+s0 cases were comparable with other LTA cases, and the values in the K2C10Ws0  
348 case were similar to the NLDN cases and improved upon the K1C10W case. The MB in the  
349 WWLLN+s0 cases were mostly positive (overestimate), which is expected because the KF  
350 scheme has more freedom to activate deep convection. The K2C10Ws0 case produced the most  
351 desirable results (domain mean MB is nearly zero) among all the cases. However, the biases  
352 associated with LTA simulations using the “NoSuppress” option are affected by both the  
353 lightning detection efficiency and the domain resolutions, which is more evident in the LTA  
354 simulations over the hemispheric domain in Section 5.

#### 355 4.2. Other Near-Surface Meteorological Variables

356 Besides precipitation, T2, water vapor mixing ratio, wind speed, and wind direction are  
357 also analyzed. As shown in Figure 4, T2 in the BASE cases has correlation coefficients over the  
358 CONUS domain and all the regions ranging from ~0.95–0.98. With LTA, the correlations for T2  
359 were further improved for all the regions, with WWLLN cases performing slightly worse than  
360 the NLDN cases. The impact of cumulus parameters on correlations was minimal for the BASE  
361 and LTA cases. However, the cumulus parameters seem to impact the biases (MB and NMB,  
362 Figures 4b,c) and errors (RMSE and NME, Figure 4d,e) in the BASE cases across all the regions,



363 and like precipitation, all the LTA cases minimized the impact of different cumulus parameter  
364 values. All the LTA cases reduced the errors (RMSE and NME) associated with T2 across all the  
365 regions, with NLDN slightly better than WWLLN. In summary, the T2 statistics were improved  
366 by using LTA, and the WWLLN cases were comparable to the NLDN cases with a slight  
367 degradation for all the regions.

368 The 2-m water vapor mixing ratios metrics (Figure 5) of the cases, in general, resemble  
369 those of T2, in that the LTA cases have slightly increased the correlation coefficients from the  
370 already well-simulated BASE cases. More spread occurs for biases (MB and NMB, Figures 5b,c)  
371 and within the BASE cases for errors (RMSE and NME, Figures 5d,e). Regional spread in these  
372 statistics is attributed to the diverse air mass types that drive large differences in the moisture  
373 content and convective activity. Even though the values were low for both errors and biases (<  
374 0.5%), using either LTA technique is an improvement over the BASE cases.

375 The cumulus parameters and LTA showed less impact on the correlations for 10-m wind  
376 speed, but the impacts on biases and errors were noticeable. All the model cases underestimate  
377 wind speed (~5–12%, depending on regions and model cases), and the cumulus parameters  
378 caused relatively large differences in the metrics of the BASE cases with both trigger and cutd  
379 options contributing most. Overall, using Trig2 with Cudt10 is most favorable in terms of biases  
380 (less underestimate) and errors (smaller errors) among the BASE cases. In all the LTA cases, the  
381 underestimation was reduced when compared to the BASE cases, and errors were reduced with  
382 negligible differences among the cases with different cumulus parameters and assimilating  
383 lightning data from the different networks. Similar behavior was observed for wind direction  
384 where only correlation coefficient, MB, and RMSE are displayed in Figure S2 because  
385 normalized metrics do not apply.



386

## 387 **5. Northern Hemispheric WRF Simulations**

388 As shown in Table 1, the model cases performed over the Northern Hemisphere are  
389 similar to those performed over the CONUS, but with LTA cases using lightning data from  
390 WWLLN that was gridded on the domain with 108-km horizontal grid spacing.

### 391 5.1. Precipitation

392 Before comparing the simulated precipitation with available observations, the examination  
393 begins with how the WRF-simulated precipitation with and without LTA compares spatially over  
394 the Northern Hemisphere. Figure 7 displays the mean daily precipitation during July 2016 from  
395 two LTA cases and two BASE cases (Trig1 and Trig2) and the corresponding differences between  
396 LTA and BASE (LTA – BASE) cases with the same trigger values, and Figure S3 presents the  
397 mean daily precipitation differences between HK1C0W and HK1C0B cases throughout 2016.  
398 Compared to the BASE cases, the LTA cases produced significantly less rainfall along the  
399 Equatorial regions but generally more rainfall away from the Equator, especially over the  
400 midlatitude land regions. Because no gauge-based observational data are available over the ocean,  
401 the IMERG precipitation for July 2016 is presented in Figure 7g with the difference plots from the  
402 base case (HK1C0B) and the LTA case (HK1C0W) being displayed in Figures 7h and 7i,  
403 respectively. Over the Equatorial regions, the precipitation simulated by the LTA cases (Figures  
404 7b and 7e) more closely resembled the IMERG precipitation than the BASE cases. The difference  
405 plots clearly indicate that the base cases significantly overestimated, and the LTA cases slightly  
406 underestimated the precipitation over large areas in the Equatorial regions. Similar results persisted  
407 throughout the year as shown in Figure S4 (the difference of mean daily precipitation by month  
408 between the base case, HK1C0B, and the IMERG product) and Figure S5 (the difference of mean



409 daily precipitation by month between the LTA case, HK1COW, and the IMERG product). Next,  
410 the WRF simulated precipitation is compared with the CPC gauge-based analysis values over land.  
411 Figure 8 displays the CPC rainfall and simulated mean daily precipitation during July 2016 along  
412 with the estimates from the LTA and BASE cases with different cumulus parameters. Since the  
413 gauge-based observational values are only available over land, the simulated values in Figure 8  
414 are only displayed over land. As shown in Figure 8, all the model cases simulated the overall  
415 spatial pattern of higher values in the tropical regions and lower values in high latitude regions.  
416 However, subtle differences existed from case to case in different regions. For example, the  
417 HK1C10B case (Figure 8d) and the HK2C10B case (Figure 8f) produced the highest and the lowest  
418 precipitation over Africa and South America (along the Mexico coast to the South American  
419 continent) within the modeling domain.

420 All the LTA cases uniformly produced larger correlation coefficients than the BASE  
421 cases (Figure 9) when and where convective activities were prevalent. In the U.S., convective  
422 activities occur during warm months (from May to September), while in Mexico and India,  
423 convection is active throughout the year. In Canada, convective activities are less frequent  
424 because of the cooler temperatures and low moisture at the high latitude. When and where  
425 convection was active, the cumulus parameters produced significant differences in modeled  
426 convective activity, as correlation coefficients are higher in the BASE cases with Trig1. Same as  
427 the simulations over the CONUS domain, the cumulus parameters had a minor impact on the  
428 correlation coefficients for the LTA cases regardless the regions. This indicates that, even with  
429 the less dense WWLLN lightning observations, using LTA improves the timing and location of  
430 deep convection.



431 RMSE were comparable for all the model cases across the selected regions (Figure 10),  
432 with the LTA cases pointing to lower values than the BASE cases at all the regions except for the  
433 U.S. where the LTA and BASE cases alternated to have slightly lower RMSE values over each  
434 other during the year. Alternatively, the MB values varied significantly among the model cases  
435 and across the regions as shown in Figure 11. One common feature is that the differences among  
436 the LTA cases were small, but two distinctly separate groups among the BASE cases in all the  
437 regions; the cases with Trig1 had always significantly greater precipitation values than the cases  
438 with Trig2. In China and Mexico, all the simulations overestimated the precipitation through the  
439 year except for small underestimate during the cool months (October–December). In India, the  
440 overestimate and underestimate were equally split among the model cases, with dramatic  
441 changes from month to month. The behavior of MB values among the model cases and through  
442 the year was more stable for the U.S. (to a lesser extent in Canada) than in other regions, in  
443 which the BASE cases with Trig1 have the best performance (MB values near zero), the BASE  
444 cases with Trig2 significantly underestimated precipitation over land during convective season,  
445 and all the LTA cases overestimated precipitation over land during the warm months. Here we  
446 offer two plausible explanations for the drastically different behaviors of the MB values  
447 associated with precipitation in different regions.

448 First, from the modeling point of view, the WRF model is widely studied and applied in  
449 North America, especially in the U.S. As a result, more accurate observation-based datasets are  
450 available to nudge WRF through FDDA (Liu et al., 2008), and all the work has led to the best  
451 performance over the U.S. for the recommended default set of convective trigger and update  
452 frequency for the cumulus scheme. Second, from the observational point of view, the CPC  
453 rainfall dataset is built upon field gauge measurements that may vary in accuracy and



454 consistency from county to county. As shown in Figure S6, the NMB values were generally in  
455 the range of -50% to 50% in the U.S. and Canada (comparable to the NMB values for the 12-km  
456 CONUS simulations against PRISM precipitation as shown in Figure 3c), but in other countries,  
457 especially during cool months, the values were up to hundreds or even thousands of percent that  
458 suggests possible few observations available in the denominator in NMB calculations. For  
459 instance, the highest NMB value in China coincided with the Spring Festival that is often a long  
460 holiday for China suggesting possible gaps for data collection.

461 We next focus on the high MB values associated with the LTA cases in the U.S.  
462 Consistent with the analysis in Figure 3b, the LTA WWLLN cases over the 12-km CONUS  
463 domain always had larger negative MB (underestimates) than the LTA NLDN cases due to the  
464 lower detection efficiency of lightning flashes in WWLLN than in NLDN. However, in the 108-  
465 km hemispheric simulations, the same WWLLN datasets produced large positive MB  
466 (overestimates) for precipitation. To understand this phenomenon, we need to first examine how  
467 the LTA method works. Because it uses a yes/no lightning indicator to trigger convection, 108-  
468 km grid spacing might be too coarse for such a simplistic approach to work. For example, one  
469 lightning strike within a 108-km grid cell will trigger deep convection, which, because of the  
470 large spatial coverage of the grid cell, can contribute to the high bias in precipitation because  
471 convective rainfall is realistically more localized. Although the KF scheme sets a fixed radius  
472 for thunderstorms (e.g., Equation 6 in Kain 2004), applying the resulting rain over the entire 108-  
473 km  $\times$  108-km grid box could partially explain the excess rainfall. This may also be explained by  
474 the fact that the convective time-scale formulation in KF scheme was originally developed at  
475 grid lengths of 20–25 km (Sims et al., 2017). A potential developmental pathway for the LTA  
476 method at these scales is to test different thresholds of the 30-min flash density to ensure



477 sufficient lightning is present to trigger deep convection. Overall, compared to the CPC rainfall,  
478 the LTA technique significantly improved the temporal and spatial correlation of convective  
479 precipitation, but the precipitation amount was overestimated over the U.S. and other regions for  
480 the 108-km modeling domain.

481 To further examine the impact of modeling domain resolutions on convective  
482 precipitation, Figure 12 displays the spatial precipitation from PRISM, CPC (regridged onto the  
483 12-km CONUS domain), and simulated precipitation from one BASE case and two LTA cases  
484 with NLDN and WWLLN data, respectively, over the 12-km CONUS domain and one LTA case  
485 over the 108-km hemispheric domain that has been regridged to the 12-km CONUS domain. As  
486 shown in Figures 12a,b, the two observation-based precipitation products, PRISM and CPC,  
487 compared well to each other, noting that the PRISM product displays more subtle granularity  
488 than the CPC product due to the large difference in spatial resolutions (4-km for PRISM versus  
489 0.5° for CPC). The overall spatial pattern of mean daily precipitation was captured by both the  
490 12-km LTA simulations (Figures 12d,e), and the 108-km LTA simulation (Figure 12f). The  
491 heaviest rainfall was centered in the OVC area in the observation-based and the simulated  
492 precipitation maps, but the shape and spread of the rain band were different. The rain band in the  
493 12-km BASE case (Figure 12c) was more spread and scattered with southwest-to-northeast  
494 orientation, while the observation-based products and the LTA cases indicated a relatively  
495 smaller area with west-east direction. Thus, the LTA cases (12-km CONUS simulations)  
496 compared better to the observation-based products spatially than the BASE case. The K2C10W  
497 case (with WWLLN) tended to produce less precipitation than the K2C10N case (with NLDN)  
498 and both observation-based products. These spatial discrepancies for precipitation in OVC  
499 between PRISM and the model cases were reflected by the unique statistical behavior as



500 displayed in Figure 3 and discussed in Section 4.1. As a likely artifact of excessively activated  
501 convection within the 108-km grid cells with a spatial scale much larger than most thunderstorm  
502 scales, the HK2C10W case indicated areas of heavy precipitation that were also shown in the  
503 observation-based products and the 12-km LTA cases at approximately same locations but with  
504 much less spatial extent. To resonate with the large discrepancies in the MB values shown in  
505 Figure 11a among the BASE cases, the precipitation from HK2C10B and HK2C10B cases is  
506 similarly displayed in Figures 12g,h. The case with Trig1 was clearly more comparable to the  
507 CONUS cases than the Trig2 case in that the precipitation was severely underestimated across  
508 the entire U.S. These hemispheric simulations amplified the impact of the trigger options on  
509 precipitation during warm months among the BASE cases, resulting in differences in daily total  
510 precipitation of up to 40% in the U.S. (Figure S6a). These results underscore the need to  
511 carefully set cumulus parameters for the KF scheme in WRF simulations.

512         The mismatch of the spatial scales between domain resolution and thunderstorms in the  
513 108-km simulations is a limitation of current LTA scheme that could be improved in future  
514 development. In addition to using lightning density to trigger convection, another option is to  
515 implement the LTA scheme in the MultiScale Kain-Fritsch (MSKF) scheme (Glotfelty et al.,  
516 2019; Zheng et al., 2016), a “scale-aware” variant of KF that refines the convective tendencies  
517 based on the grid spacing used in the simulation.

## 518 5.2. Impact on Other Meteorological Variables

519         The impact of the cumulus parameters and LTA scheme on near-surface meteorological  
520 variables of the 108-km hemispheric simulations are evaluated like the 12-km CONUS  
521 simulations. However, due to the lack of observation data beyond North America, the analysis is  
522 mainly focused on the U.S. regions, but all the available data within the hemispheric domain is



523 collectively referred to as “ALL” regardless of where the data originated. Affected by the coarser  
524 domain resolution, all the statistical measures for T2 (Figure 13) from the hemispheric  
525 simulations indicated degradations in model performance relative to the 12-km CONUS domain  
526 (Figure 4). As in the CONUS simulations, the LTA cases increased correlation coefficients and  
527 decreased errors (RMSE and NME) compared to the BASE cases. Like the CONUS simulations,  
528 the cumulus parameters minimally affected the LTA cases, while significant deviations were  
529 produced among the BASE cases. Unlike the CONUS simulations where both trigger and cutd  
530 contributed to T2 differences, the large differences among the BASE cases for the hemispheric  
531 simulations were attributed to the trigger options. Though all the cases tended to underestimate  
532 T2 (contrary to the CONUS simulations where T2 was generally overestimated), among the  
533 BASE cases, greater underestimates were associated with Trig1 than Trig2. The LTA cases  
534 uniformly underestimated T2 consistent with the Trig1 BASE cases. The performance of  
535 hemispheric simulations for 2-m water vapor mixing ratio (Figure 14) resembles T2 in the  
536 comparison to the CONUS simulations (Figure 5), which produced smaller correlation  
537 coefficients and larger errors and biases (mainly overestimates for both CONUS and hemispheric  
538 simulations). Without exception, the LTA cases consistently performed better in terms of  
539 correlation coefficients and errors than the BASE cases. However, different from other  
540 meteorological variables, the MB and NMB associated with water vapor mixing ratio are  
541 affected by both cumulus parameters (trigger and cutd) for all the model cases (both BASE cases  
542 and LTA cases). The LTA cases with Trig1 performed better than the cases with Trig2, and with  
543 the same trigger value, cutd=0 is preferable to cutd=10; however, for the BASE cases, it was the  
544 opposite, though with smaller differences. At the 108-km grid spacing, the 10-m wind speed



545 (Figure S7) and wind direction (not shown) statistics were comparable among the cumulus  
546 parameters and the application of LTA.

547

## 548 **6. Discussion and Recommendations**

549 This study corroborated that the simple observation-based LTA scheme implemented in  
550 Heath et al. (2016) improved WRF simulated precipitation and other near-surface meteorological  
551 variables as evidenced by the simulations over multiple spatial scales and over a longer test  
552 period. Testing on a 12-km CONUS domain using lightning flashes from WWLLN instead of  
553 NLDN slightly reduced the correlation coefficients and locally increased errors due to the lower  
554 detection efficiency of WWLLN. The update of the LTA technique reduced the underestimate of  
555 precipitation that was often reported in the application of WRF simulations conducted over the  
556 CONUS domain (U.S. EPA, 2019). Changing lightning flash data from NLDN to WWLLN  
557 resulted in additional underestimate of precipitation due to fewer lightning flashes in WWLLN  
558 than the NLDN dataset. However, when the WWLLN data was used in the hemispheric  
559 simulations, the model performance for precipitation over the Equatorial regions was  
560 significantly improved from significant overestimation in the base cases to slight  
561 underestimation in the LTA cases, and the precipitation over land was generally overestimated  
562 during the convective season for almost all the selected regions, especially over North America.

563 The application of LTA in the hemispheric simulations with a 108-km domain exposed a  
564 shortcoming of this simple LTA scheme. When the model grid cell is substantially larger than  
565 most thunderstorm scales (Murphy and Konrad II, 2005), over-triggering of convection within the  
566 entire grid cell leads to overestimated precipitation. With the current LTA implementation and  
567 the high lightning detection efficiency network, such as NLDN, the 12-km grid spacing is  
568 suitable for LTA because thunderstorms often have a radial distance of 1–10 km. When lightning



569 data from low detection efficiency networks (such as WWLLN) are used over finer resolution  
570 domains ( $\leq 12$  km), the “NoSuppress” option with LTA could balance increasing precipitation  
571 while maintaining reasonable levels of uncertainty in the other variables for a more holistic  
572 model evaluation. The effect of domain resolution on precipitation simulation with LTA  
573 portends further development and improvement of the LTA technique. Two potential  
574 developmental directions are to alter values of lightning flash density to trigger deep convection  
575 and/or to implement the LTA scheme in the MSKF scheme in WRF to adapt to different  
576 simulation scales. Preliminary experimentation on the 108-km scale (not shown) suggests that  
577 MSKF could improve these comparisons with observations (compared to the KF scheme  
578 presented here), including better cloud and precipitation fields (Hogrefe et al., 2021).

579 The experiment of cumulus parameters (trigger and *cutd*) associated with the KF scheme was  
580 performed for both the CONUS and hemispheric WRF simulations. Results revealed several key  
581 behaviors in both the BASE case simulations and LTA case simulations. First, the BASE case  
582 simulations were sensitive to both trigger and *cutd* options over the CONUS domain, but only  
583 trigger options produced significant variations for the hemispheric simulations. Second, the  
584 impact of the cumulus parameters on LTA cases was insignificant for both modeling domains.  
585 Separately, the original LTA technique as described in Heath et al. (2016) showed influence  
586 from the cumulus parameters on the LTA cases (Figure S8), but after implementing the updates  
587 described in Section 2, the fluctuations among the LTA cases were significantly reduced. Third,  
588 the most pronounced impact of cumulus parameters was on the amount of precipitation in the  
589 BASE cases. The Trig1 option generated up to a 10% overestimate of month-mean daily  
590 precipitation over the CONUS with *cutd*=0 and an additional 10–15% overestimate with *cutd*=10  
591 during July 2016. With Trig2, the simulated precipitation became underestimated by about 10–



592 15%, with the *cudt* contributing to ~5% difference; *Cudt10* had less underestimate than *Cudt0*.  
593 However, over the hemispheric domain, only the trigger option dramatically affected simulated  
594 precipitation; during the summer months (June, July, and August), the *Trig2* cases  
595 underestimated the mean daily precipitation by up to 40% more than the *Trig1* cases that  
596 matched the observation-based precipitation products within 10%. In summary, without LTA,  
597 the recommended default values (*trigger=1* and *cudt=0*) by WRF documentation remain the best  
598 option for both the CONUS and hemispheric simulations to achieve the best model performance,  
599 especially for North America, and with LTA, all the options performed equally well.

600 As one of the most prominent meteorological models, WRF has been widely used in a variety  
601 of applications from regional to global scales and from weather and climate studies to air  
602 pollution transport in air quality forecast and regulatory compliances. It is important to improve  
603 the convective processes to have more accurate precipitation and other meteorological fields with  
604 more resources being available including observational datasets, computing capability, and  
605 advanced scheme development. Observation-based data assimilation has been historically proven  
606 to be one of the most effective methods to improve model's performance in time and space. This  
607 research is emerging to consider and use the lightning observations that have become available in  
608 various formats and scales in the past decades to improve convection simulations through LTA.  
609 Additional networks of lightning observations and more detailed properties associated with the  
610 process of lightning discharge are becoming available (such as the scope and strength of  
611 lightning energy level and the separation of cloud-to-ground and inter- or intra-cloud strikes  
612 being more accurately quantified, especially with the available satellite lightning products from  
613 Geostationary Lightning Mapper (GLM) detection systems borne on the GOES-16 and -17



614 satellites (Goodman et al., 2013)). Accordingly, lightning assimilation techniques will continue

615 to evolve and build upon the research presented here.

616



617 **Code and data availability**

618 The WRF model is available for download through the WRF website (<http://www.wrf->  
619 [model.org/index.php](http://www.wrf-model.org/index.php)). The LTA code is not publicly available yet but interested users can  
620 contact the corresponding author to acquire the source code. The raw lightning flash observation  
621 data can be purchased through Vaisala Inc. ([https://](https://www.vaisala.com/en/products/systems/lightning-detection)  
622 [www.vaisala.com/en/products/systems/lightning-detection](https://www.vaisala.com/en/products/systems/lightning-detection)), and the WWLLN raw data are also  
623 available for purchase at <http://wwlln.net>. The immediate data except the lightning flash data  
624 behind the figures are available from doi: <https://doi.org/10.5281/zenodo.6493145>.

625

626 **Author contributions.** DK conceptualized the study, performed the model simulation and data  
627 curation, carried out the analysis, and wrote the paper. NH developed the mechanism and  
628 software and wrote the paper. RG prepared the scripts for model simulations and data analysis  
629 and edited the paper. TS supervised the research, provided resources, and edited the paper. JP  
630 edited the paper.

631

632 **Competing interests.** The authors declare that they have no conflict of interest.

633

634 **Disclaimer:** This paper has been subjected to an EPA review and approved for publication. The  
635 views expressed here are those of the authors and do not necessarily reflect the views or policies  
636 of the U.S. Environmental Protection Agency (EPA).

637

638 **Acknowledgement:**

639 We thank Jerry Herwehe and Kiran Alapaty at the EPA for reviewing the paper and providing valuable  
640 comments and suggestions. PRISM Precipitation data for the United States are retrieved from  
641 [https://climatedataguide.ucar.edu/climate-data/prism-high-resolution-spatial-climate-data-united-states-](https://climatedataguide.ucar.edu/climate-data/prism-high-resolution-spatial-climate-data-united-states-maxmin-temp-dewpoint)  
642 [maxmin-temp-dewpoint](https://climatedataguide.ucar.edu/climate-data/prism-high-resolution-spatial-climate-data-united-states-maxmin-temp-dewpoint) and the CPC Global Unified Precipitation data provided by the  
643 NOAA/OAR/ESRL PSL, Boulder, Colorado, USA, from their Web site  
644 at <https://psl.noaa.gov/data/gridded/data.cpc.globalprecip.html>. The IMERG data were provided by the  
645 NASA/Goddard Space Flight Center's Precipitation Measurement Missions (PMM) Science Team and  
646 Precipitation Processing System (PPS), which develop and compute the IMERG as a contribution to  
647 GPM, and archived at the NASA GES DISC.

648



649 **References**

- 650 Abarca, S. F., Corbosiero, K. L., and Galarneau Jr., T. J.: An evaluation of the Worldwide Lightning  
651 Location Network (WWLLN) using the National Lightning Detection Network (NLDN) as ground  
652 truth, *J. Geophys. Res.*, 115, D18206, doi:10.1029/2009JD013411, 2010.
- 653 Appel, K. W., Gilliam, R. C., Davis, N., Zubrow, A., and S. C. Howard, S. C.: Overview of the  
654 Atmospheric Model Evaluation Tool (AMET) v1.1 for evaluating meteorological and air quality  
655 models, *Environ. Modell. Software*, 26, 434–443, doi:10.1016/j.envsoft.2010.09.007, 2011.
- 656 Appel, K. W., Bash, J. O., Fahey, K. M., Foley, K. M., Gilliam, R. C., Hogrefe, C., Hutzell, W. T., Kang,  
657 D., Mathur, R., Murphy, B. N., Napelenok, S. L., Nolte, C. G., Pleim, J. E., Pouliot, G. A., Pye, H.  
658 O., Ran, L., Roselle, S. J., Sarwar, G., Schwede, D. B., Sidi, F. L., Spero, T. L., and Wong, D. C.: The  
659 Community Multiscale Air Quality (CMAQ) model versions 5.3 and 5.3.1: system updates and  
660 evaluation, *Geosci. Model Dev.*, 14, 2867–2897, <https://doi.org/10.5194/gmd-14-2867-2021>, 2021.
- 661 Asong, Z. E., Razavi, S., Wheeler, H. S., and Wong, J. S.: Evaluation of Integrated Multisatellite  
662 Retrievals for GPM (IMERG) over Southern Canada against Ground Precipitation Observations: A  
663 Preliminary Assessment, *J. Hydrometeorology*, 18, 1033–1050, [https://doi.org/10.1175/JHM-D-16-  
664 0187.1](https://doi.org/10.1175/JHM-D-16-0187.1), 2017.
- 665 Bruning, E. C., Weiss, S. A., and Calhoun, K. M.: Continuous variability in thunderstorm primary  
666 electrification and an evaluation of inverted-polarity terminology, *Atmos. Res.*, 135–136, 274–284,  
667 doi:10.1016/j.atmosres.2012.10.009, 2014.
- 668 Burgess, R. E.: Assessment of the World Wide Lightning Location Network (WWLLN) detection  
669 efficiency by comparison to the Lightning Imaging Sensor (LIS), *Q. J. R. Meteorol. Soc.* 143: 2809–  
670 2817, doi:10.1002/qj.3129, 2017.
- 671 Fierro, A. O., Mansell, E. R., Ziegler, C. L., and MacGorman, D. R.: Application of a lightning data  
672 assimilation technique in the WRFARW model at cloud-resolving scales for the tornado outbreak of  
673 24 May 2011, *Mon. Weather Rev.*, 140, 2609–2627, 2012.



- 674 Fierro, A. O., Clark, A., Mansell, E. R., MacGorman, D. R., Dembek, S. R., and Ziegler, C. L.: Impact of  
675 storm-scale lightning data assimilation on WRF-ARW precipitation forecasts during the 2013 warm  
676 season over the contiguous United States, *Mon. Weather Rev.*, 143, 757–777, 2015.
- 677 Finney, D. L., Doherty, R. M., Wild, O., Huntrieser, H., Pumphrey, H. C., and Blyth, A. M.: Using cloud  
678 ice flux to parametrise large-scale lightning, *Atmospheric Chemistry and Physics*, 14 (23),  
679 12,665–12,682, doi:10.5194/acp-14-12665-2014, 2014.
- 680 Gan, R., Yang, Y., Xie, Q., Lin, E., Wang, Y., and Liu, P.: Assimilation of Radar and Cloud-to-Ground  
681 Lightning Data Using WRF-3DVar Combined with the Physical Initialization Method—A Case  
682 Study of a Mesoscale Convective System. *J. Meteorol. Res.* 35, 329–342.  
683 <https://doi.org/10.1007/s13351-021-0092-4>, 2021.
- 684 Giannaros, T. M., Kotroni, V., and Lagouvardos, K.: WRF-LTNGDA: A lightning data assimilation  
685 technique implemented in the WRF model for improving precipitation forecasts, *Environ. Modell.*  
686 *Software*, 76, 54–68, 2016.
- 687 Glotfelty, T., Alapaty, K., He, J., Hawbecker, P., Song, X., and Zhang, G.: The Weather Research and  
688 Forecasting Model with Aerosol–Cloud Interactions (WRF-ACI): Development, evaluation, and  
689 initial application, *Mon. Wea. Rev.*, 147, 1491–1511, doi:10.1175/MWR-D-18-0267.1, 2019.
- 690 Goodman, S. J., Blakeslee, R. J., Koshak, W. J., Mach, D., Baiely, J., Buechler, D., Carey, L., Schultz, C.,  
691 Bateman, M., McCaul Jr., E., and Stano G.: The GOES-R Geostationary Lightning Mapper (GLM),  
692 *Atmos. Res.*, 125–126, 34–49, doi: 10.1016/j.atmosres.2013.01.006, 2013.
- 693 Heath, N. K., Pleim, J. E., Gilliam, R. C., and Kang, D.: A simple lightning assimilation technique for  
694 improving retrospective WRF simulations, *J. Adv. Model. Earth Syst.*, 8, 1806–1824,  
695 <https://doi.org/10.1002/2016MS000735>, 2016.
- 696 Hogrefe, C., Gilliam, R., Mathur, R., Henderson, B., Sarwar, G., Appel, K. W., Pouliot, G., Willison, J.,  
697 Miller, R., Vukovich, J., Eyth, A., Talgo, K., Allen, C., and Foley, K.: CMAQv5.3.2 ozone  
698 simulations over the Northern Hemisphere: model performance and sensitivity to model  
699 configuration. 20th Annual CMAS Conference, November 1–5, 2021, Virtual, 2021.



- 700 Huffman, G. J., Adler, R. F., and Nelkin, E. J.: Integrated Multi-satellite Retrievals for GPM (IMERG)  
701 technical documentation. NASA/GSFC Code 612 Tech. Doc., 48 pp. [Available online at  
702 [http://pmm.nasa.gov/sites/default/files/document\\_files/IMERG\\_doc.pdf](http://pmm.nasa.gov/sites/default/files/document_files/IMERG_doc.pdf)], 2015.
- 703 Kain, J. S.: The Kain-Fritsch convective parameterization: An update, *J. Appl. Meteorol.*, 43(1), 170–181,  
704 doi:10.1175/1520-0450(2004)043<0170:TKCPAU>2.0.CO;2, 2004.
- 705 Kain, J.S. and Fritsch, J. M.: A one-dimensional entraining/detraining plume model and its application in  
706 convective parameterization, *J. Atmos. Sci.*, 47, pp. 2784-280, 1990.
- 707 Kain, J.S. and Fritsch, J. M.: Convective parameterization for mesoscale models: the Kain–Fritsch  
708 scheme, *The Representation of Cumulus Convection in Numerical Models*, Meteor. Monogr., No. 46,  
709 Amer. Meteor. Soc., pp. 165-170, 1993.
- 710 Kang, D., Mathur, R., Pouliot, G. A., Gilliam, R. C., and Wong, D. C.: Significant ground-level ozone  
711 attributed to lightning-induced nitrogen oxides during summertime over the Mountain West States,  
712 *npj Climate and Atmospheric Science* 3, doi: 10.1038/s41612-020-0108-2, 2020.
- 713 Kang, D., Pickering, K., Allen, D., Foley, K., Wong, D., Mathur, R., and Roselle, S.: Simulating  
714 Lightning NO Production in CMAQv5.2: Evolution of Scientific Updates, *Geosci. Model Dev.* 12,  
715 3071-3083, <https://doi.org/10.5194/gmd-12-3071-2019>, 2019a.
- 716 Kang, D., Foley, K., Mathur, R., Roselle, S., Pickering, K., and Allen, D.: Simulating Lightning NO  
717 Production in CMAQv5.2: Performance Evaluations, *Geosci. Model Dev.* 12, 4409–4424,  
718 <https://doi.org/10.5194/gmd-12-4409-2019>, 2019b.
- 719 Lagouvardos, K., Kotroni, V., Defer, E., and Bousquet, O.: Study of a heavy precipitation event over  
720 southern France, in the frame of HYMEX project: Observational analysis and model results using  
721 assimilation of lightning, *Atmos. Res.*, 134, 45–55, 2013.
- 722 Liu, Y., Warner, T. T., Bowers, J. F., Carson, L. P., Chen, F., Clough, C. A., Davis, C.A., Egeland, C. H.,  
723 Halvorson, S. F., Huck Jr., T. W., Lachapelle, L., Malone, R. E., Rife, D. L., Sheu, R. -S., Swerdlin,  
724 S. P., and Weingarten, D. S.: The operational mesogamma-scale analysis and forecast system of the



- 725 U. S. Army Test and Evaluation Command. Part 1: Overview of the modeling system, the forecast  
726 products, *J. Appl. Meteorol. Climatol.*, 47, 1077–1092, 2008.
- 727 Lopez, P.: A lightning parameterization for the ECMWF Integrated Forecasting System, *Monthly*  
728 *Weather Review*, 144 (9), 30573075, doi:10.1175/mwr-d-16-0026.1, 2016.
- 729 Ma, L.-M., and Tan, Z. M.: Improving the Behavior of the Cumulus Parameterization for Tropical  
730 Cyclone Prediction: Convection Trigger. *Atmospheric Research*, 92, 190-211.  
731 <https://doi.org/10.1016/j.atmosres.2008.09.022>, 2009.
- 732 Mach, D. M., Christian, H. J., Blakeslee, R. J., Boccipio, D. J., Goodman, S. J., and Boeck, W. L.:  
733 Performance assessment of the Optical Transient Detector and Lightning Imaging Sensor, *J. Geophys.*  
734 *Res.*, 112, D09210, doi:10.1029/2006JD007787, 2007.
- 735 Mansell, E. R., Ziegler, C. L., and MacGorman, D. R.: A lightning data assimilation technique for  
736 mesoscale forecast models, *Mon. Weather Rev.*, 135, 1732–1748, doi:10.1175/MWR3387.1, 2007.
- 737 Marchand, M. R., and Fuelberg, H. E.: Assimilation of lightning data using a nudging method involving  
738 low-level warming, *Mon. Weather Rev.*, 142, 4850–4871, doi:10.1175/MWR-D-14-00076.1., 2015.
- 739 Murphy, M. J., Cramer, J. A., and Said, R. K.: Recent history of upgrades to the U.S. National Detection  
740 Network, *J. Atmos. Ocean. Tech.*, 38, 573-581, doi:10.1175/JTECH-D-19-0215.1, 2021.
- 741 Murphy, M. S., and Konrad II, C. E.: Spatial and temporal patterns of thunderstorm events that produce  
742 cloud-to-ground lightning in the interior southeastern United States, *Monthly Weather Review*, 133,  
743 1417-1420, 2005.
- 744 Preston, A. D., and Fuelberg, H. E.: Improving lightning cessation guidance using polarimetric radar data,  
745 *Weather Forecasting*, 30, 308–328, doi:10.1175/WAF-D-14-00031.1, 2013.
- 746 Price, C., and Rind D.: A simple lightning parameterization for calculating global lightning distributions,  
747 *Journal of Geophysical Research: Atmospheres*, 97 (D9), 99199933, doi:10.1029/92jd00719, 1992.
- 748 Rogers, R. F., Fritsch, J. M., and Lambert, W. C.: A simple technique for using radar data in the dynamic  
749 initialization of a mesoscale model, *Mon. Weather Rev.*, 128, 2560–2574, 2000.



750 Romps, D. M., Seeley, J. T., Vollaro, D., and Molinari, J.: Projected increase in lightning strikes in the  
751 United States due to global warming, *Science*, 346 (6211), 851854, doi:10.1126/science.1259100,  
752 2014.

753 Rudlosky, S. D., and Shea, D. T.: Evaluation WWLLN performance relative to TRMM/LIS, *Geophys.*  
754 *Res. Lett.*, 40, 2344-2348, doi:10.1002/grl.50428, 2013.

755 Sims, A. P., Alapaty, K., and Raman, S.: Sensitivities of Summertime Mesoscale Circulations in the  
756 Coastal Carolinas to Modifications of the Kain-Fritsch Cumulus Parameterization, *Mon. Wea. Rev.*,  
757 145, 4381-4399, doi:10.1175/MWR-D-16-0047.1, 2017.

758 Skamarock, W. C., and Klemp, J. B.: A time-split nonhydrostatic atmospheric model, *Journal of*  
759 *Computational Physics*, 227, 3465-3485, doi:10.1016/j.jcp.2007.01.037, 2008.

760 Stolzenburg, M., and Marshall, T. C.: Electric field and charge structure in lightning-producing clouds,  
761 *Lightning: Principles, Instruments and Applications*, H.-D. Betz, U. Schumann, P. Laroche (Eds.),  
762 641 pp., Springer, doi:10.1007/978-1-4020-9079-0\_3, 2009.

763 U.S. EPA: Meteorological Model Performance for Annual 2016 Simulation WRF v3.8, EPA-454/R-19-  
764 010, [https://www.epa.gov/sites/default/files/2020-10/documents/met\\_model\\_performance-](https://www.epa.gov/sites/default/files/2020-10/documents/met_model_performance-2016_wrf.pdf)  
765 [2016\\_wrf.pdf](https://www.epa.gov/sites/default/files/2020-10/documents/met_model_performance-2016_wrf.pdf), 2019.

766 Zheng, Y., Alapaty, K., Herwehe, J. A., Del Genio, A. D., and Niyogi, D.: Improving high-  
767 resolution weather forecasts using the Weather Research and Forecasting (WRF) Model with  
768 an updated Kain–Fritsch scheme, *Mon. Wea. Rev.*, 144, 833–860, doi:10.1175/MWR-D-15-  
769 0005.1, 2016.

770



771

772 **Table 1. Model Cases (N/A: Not Applicable)**

773

Case Name	trigger (K1 or K2)	cutd (C0 or C10)	LTA (B, N, W)	Network	Domain
K1C0B	1	0	NO	N/A	CONUS
K1C10B	1	10	NO	N/A	CONUS
K2C0B	2	0	NO	N/A	CONUS
K2C10B	2	10	NO	N/A	CONUS
K1C0N	1	0	YES	NLDN	CONUS
K1C10N	1	10	YES	NLDN	CONUS
K2C0N	2	0	YES	NLDN	CONUS
K2C10N	2	10	YES	NLDN	CONUS
K1C0W	1	0	YES	WWLLN	CONUS
K1C10W	1	10	YES	WWLLN	CONUS
K2C0W	2	0	YES	WWLLN	CONUS
K2C10W	2	10	YES	WWLLN	CONUS
HK1C0B	1	0	NO	N/A	Hemisphere
HK1C10B	1	10	NO	N/A	Hemisphere
HK2C0B	2	0	NO	N/A	Hemisphere
HK2C10B	2	10	NO	N/A	Hemisphere
HK1C0W	1	0	YES	WWLLN	Hemisphere
HK1C10W	1	10	YES	WWLLN	Hemisphere
HK2C0W	2	0	YES	WWLLN	Hemisphere
HK2C10W	2	10	YES	WWLLN	Hemisphere

774

775

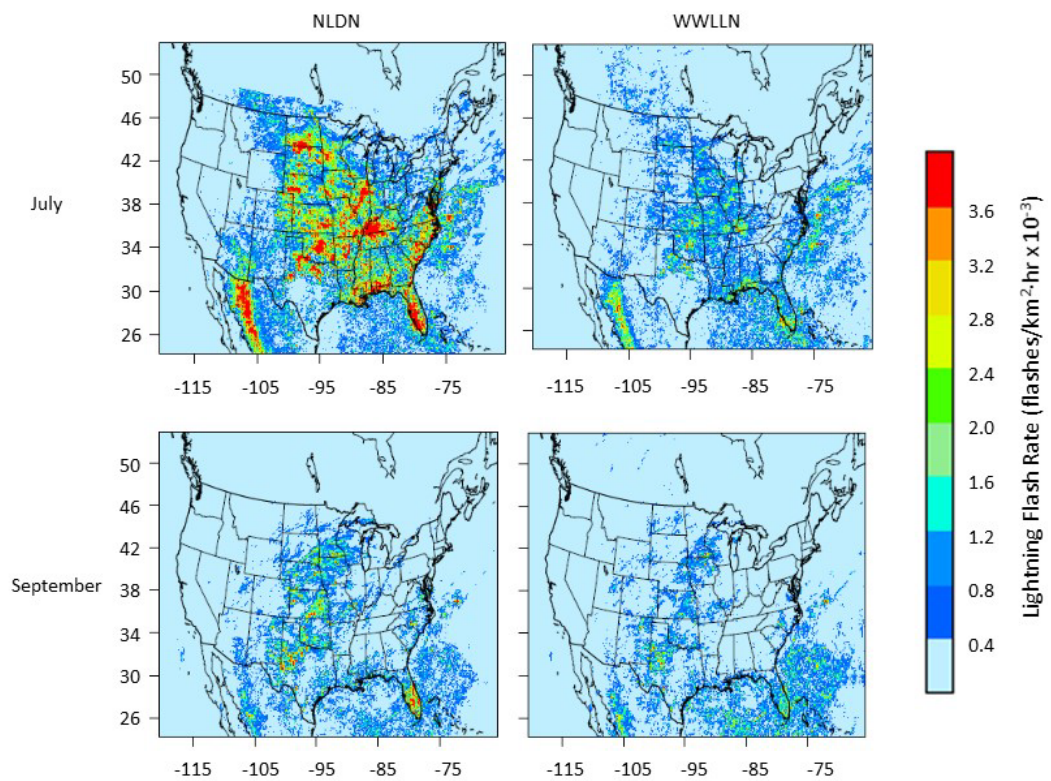
776

777

778



779



780

781 **Figure 1.** The mean hourly lightning flash rate from NLDN and WWLLN over the 12km

782 CONUS domain in July and September 2016.

783

784

785

786

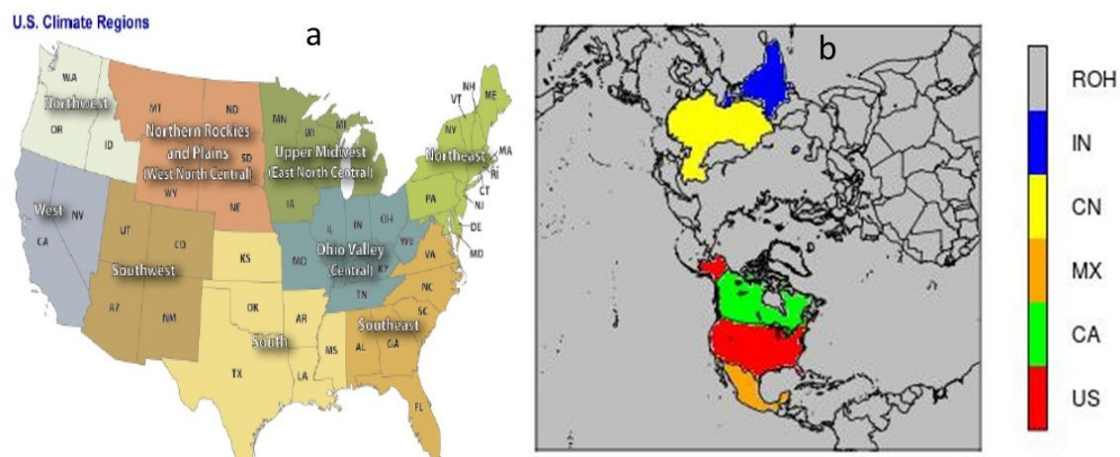
787

788



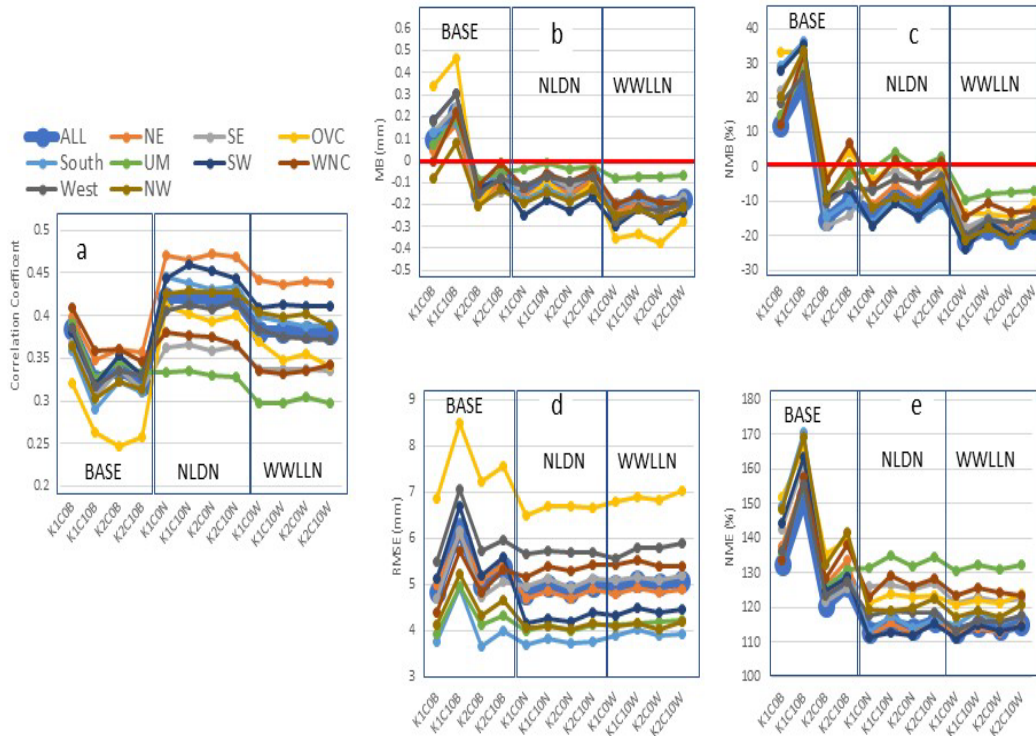
789

790



791

792 **Figure 2.** Analysis Regions (Countries), a. the climate regions in the CONUS, and b. the  
793 countries over the northern hemisphere – US: United States; CA: Canada; MX: Mexico; CN:  
794 China; IN: India; ROH: Other countries/regions except the five specific countries in the  
795 hemispheric domain. The U.S. climate regions are: Northeast (NE), Southeast (SE), Ohio Valley  
796 Central (OVC), Upper Midwest (UM), South, West North Central (WNC), Southwest (SW),  
797 Northwest (NW), and West.



798

799

**Figure 3.** Monthly mean statistics for precipitation from BASE and LTA simulations

800

comparing to the values from PRISM for the modeling domain and the climatological

801

regions over the CONUS, respectively, during July 2016: a) correlation coefficient, b) MB,

802

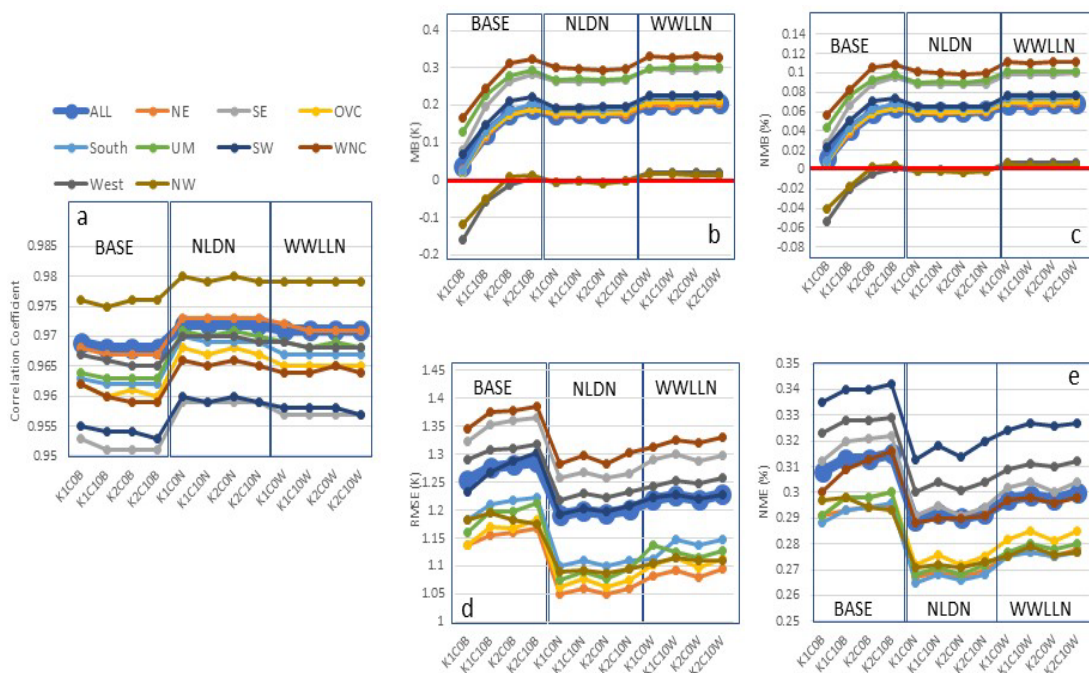
c) NMB, d) RMSE, and e) NME. In each plot, there are three sets of simulations (BASE,

803

LTA with NLDN, and LTA with WWLLN) and each having four cases from the

804

combinations of cumulus parameters.



805

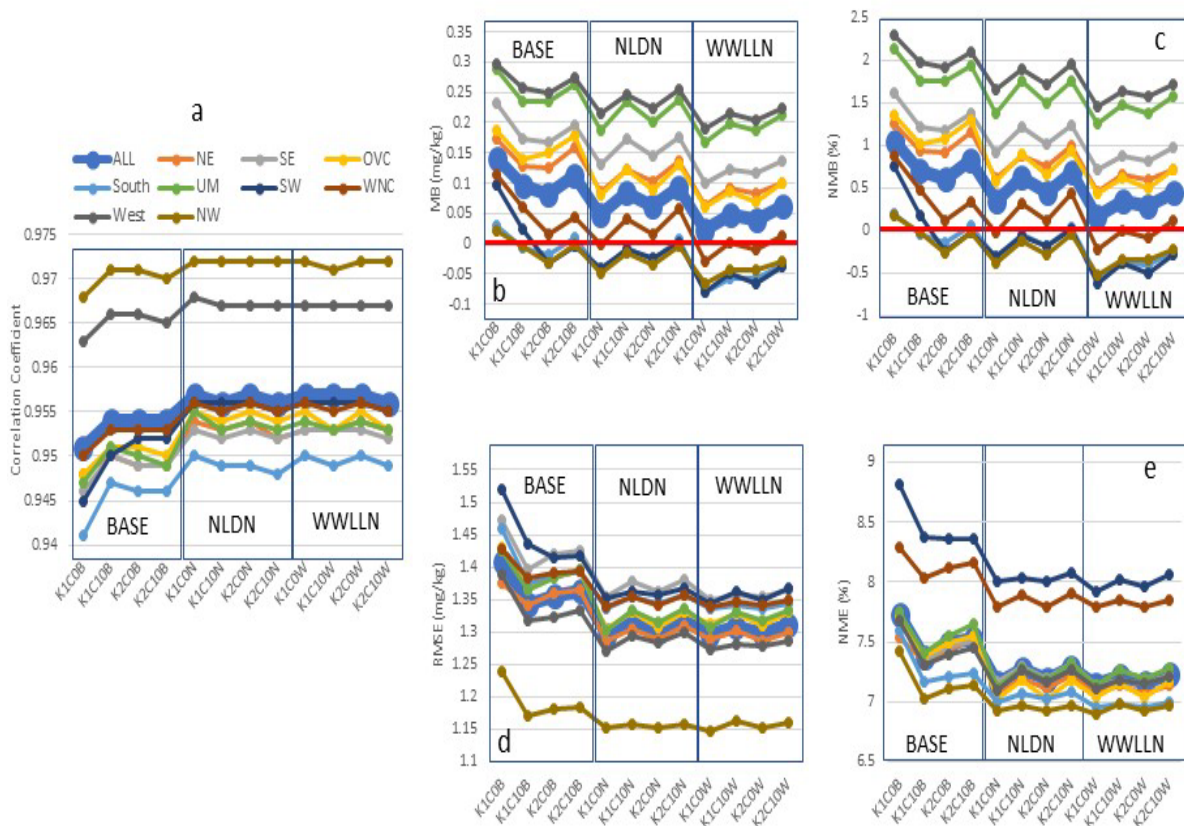
806

807

808

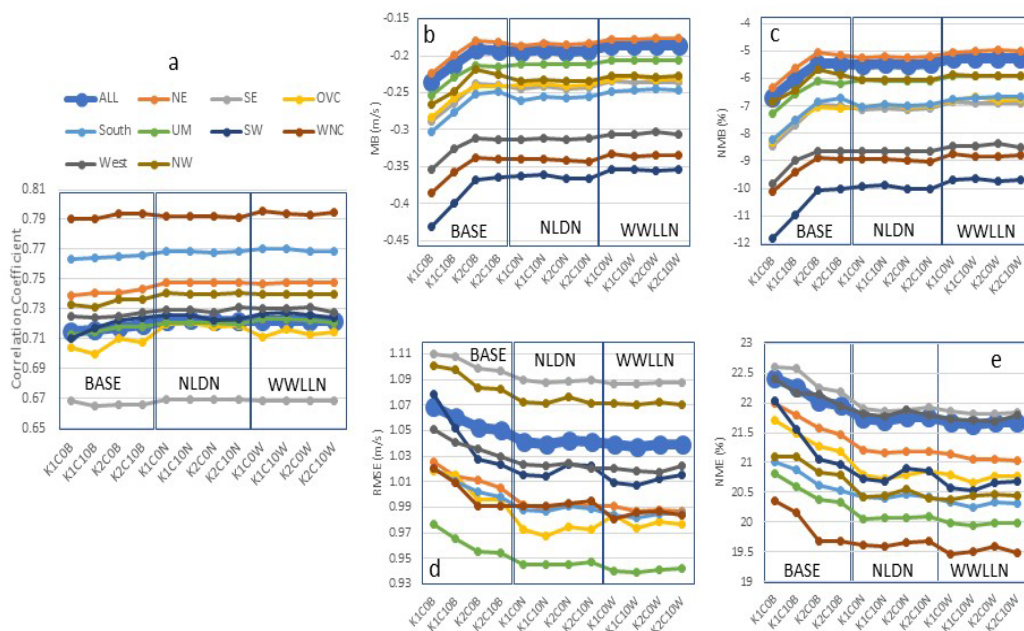
809

**Figure 4.** Same as Figure 3, but for 2-m temperature (T2) in that the simulated T2 values are paired with observations from NCEI’s land-based stations in time and space (hourly mean values).



810

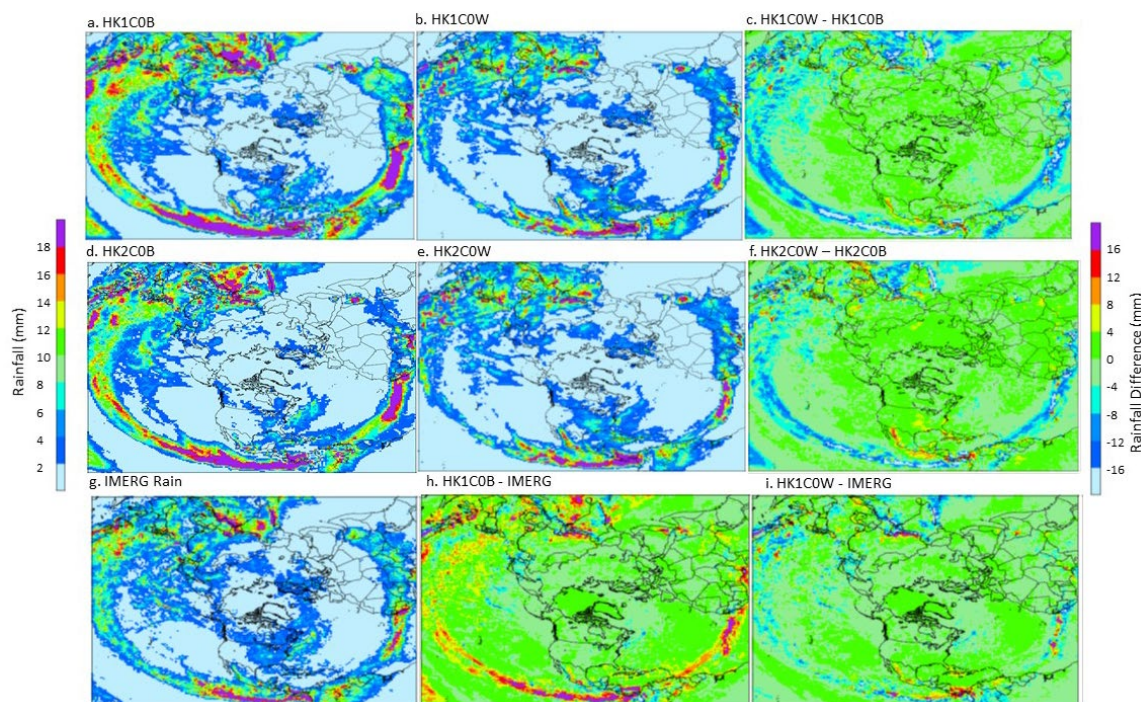
811 **Figure 5.** Same as Figure 4, but for 2-m water vapor mixing ratio.



812

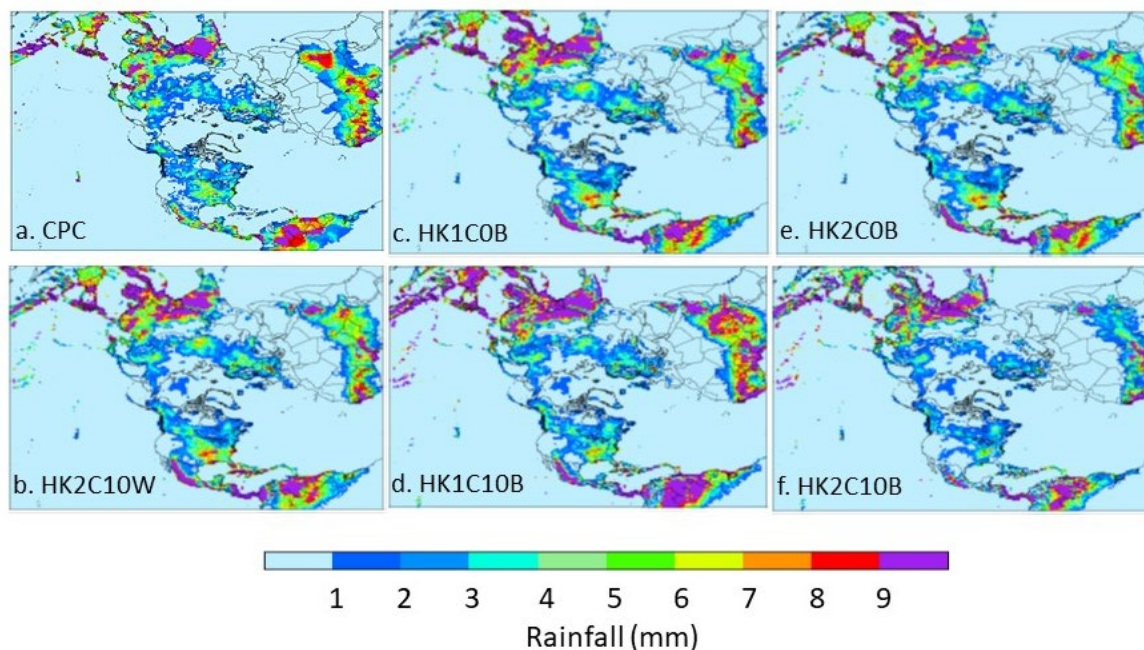
813 **Figure 6.** Same as Figure 4, but for 10-m wind speed.

814



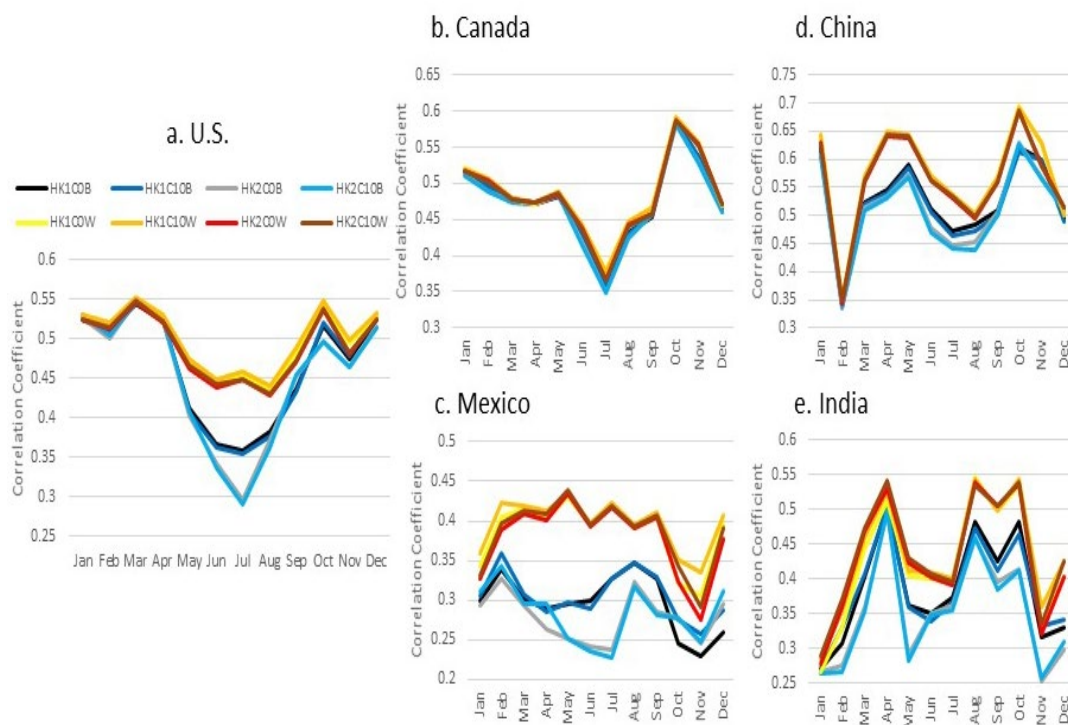
815

816 **Figure 7.** The mean daily rainfall during July 2016 simulated by base model cases (a. HK1C0B  
817 and d. HK2C0B), LTA cases (b. HK1C0W and e. HK2C0W), and the satellite GPM  
818 produced rainfall (g), and the differences between the LTA and BASE cases (c.  
819 HK1C0W – HK1C0B and f. HK2C0W – HK2C0B) and between the simulated cases and  
820 satellite IMERG products (h. HK1C0B – IMERG and i. HK1C0W – IMERG). Note that  
821 the left legend applies to the rain maps (a, b, d, e, and g), and the right legend applies to  
822 the difference plots (c, f, h, and i).



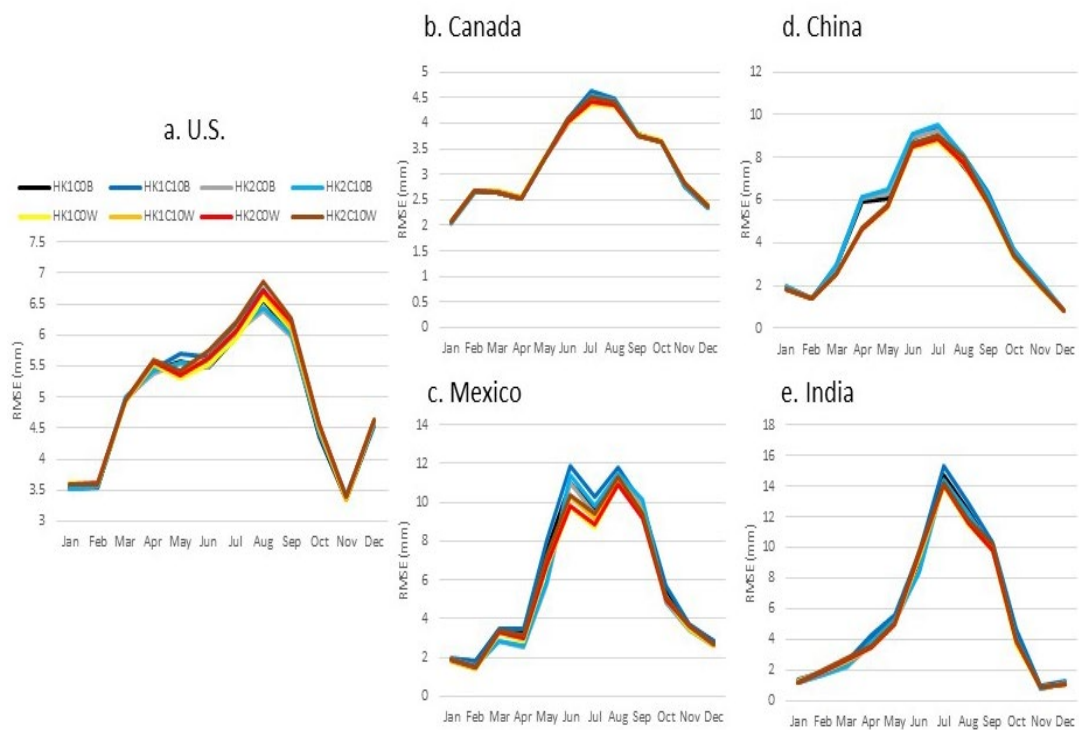
823

824 **Figure 8.** CPC rainfall (a) and simulated (b-f) mean daily precipitation during July 2016 over the  
825 hemispheric domain. The LTA configuration is represented by one case (b. HK2C10W) since all  
826 the LTA cases with different cumulus parameters produced similar results. All BASE cases are  
827 shown here (c-f) because the cumulus parameters do impact the simulated precipitation when not  
828 using LTA.



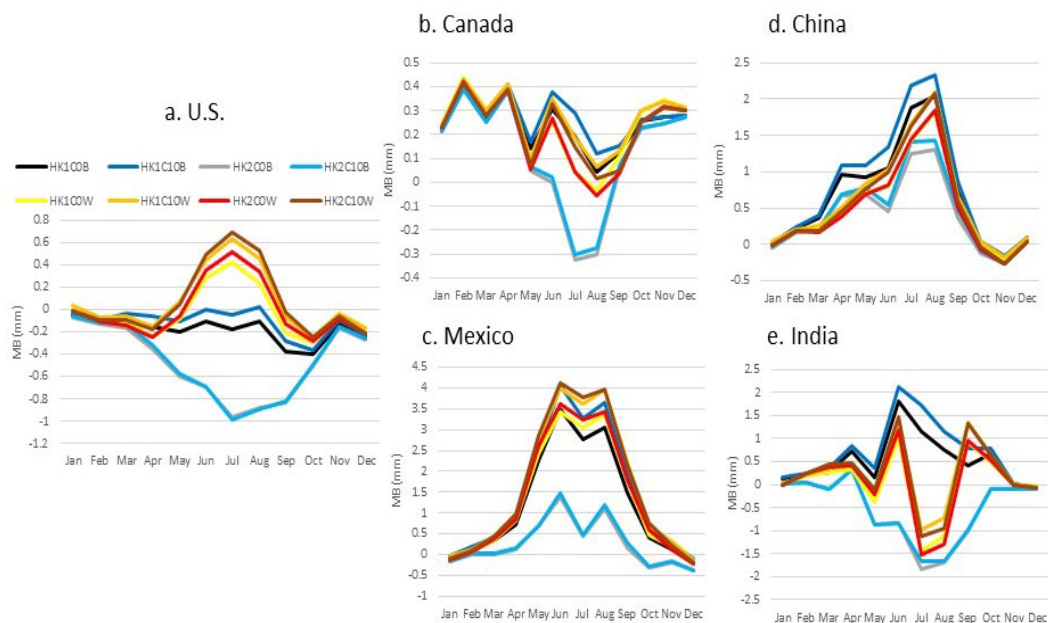
829

830 **Figure 9.** The monthly correlation coefficient between CPC and simulated precipitation in  
 831 selected countries: a. United States, b. Canada, c. Mexico, d. China, and e. India. Note  
 832 that all the BASE cases are plotted in cool colors and LTA cases in warm colors.  
 833



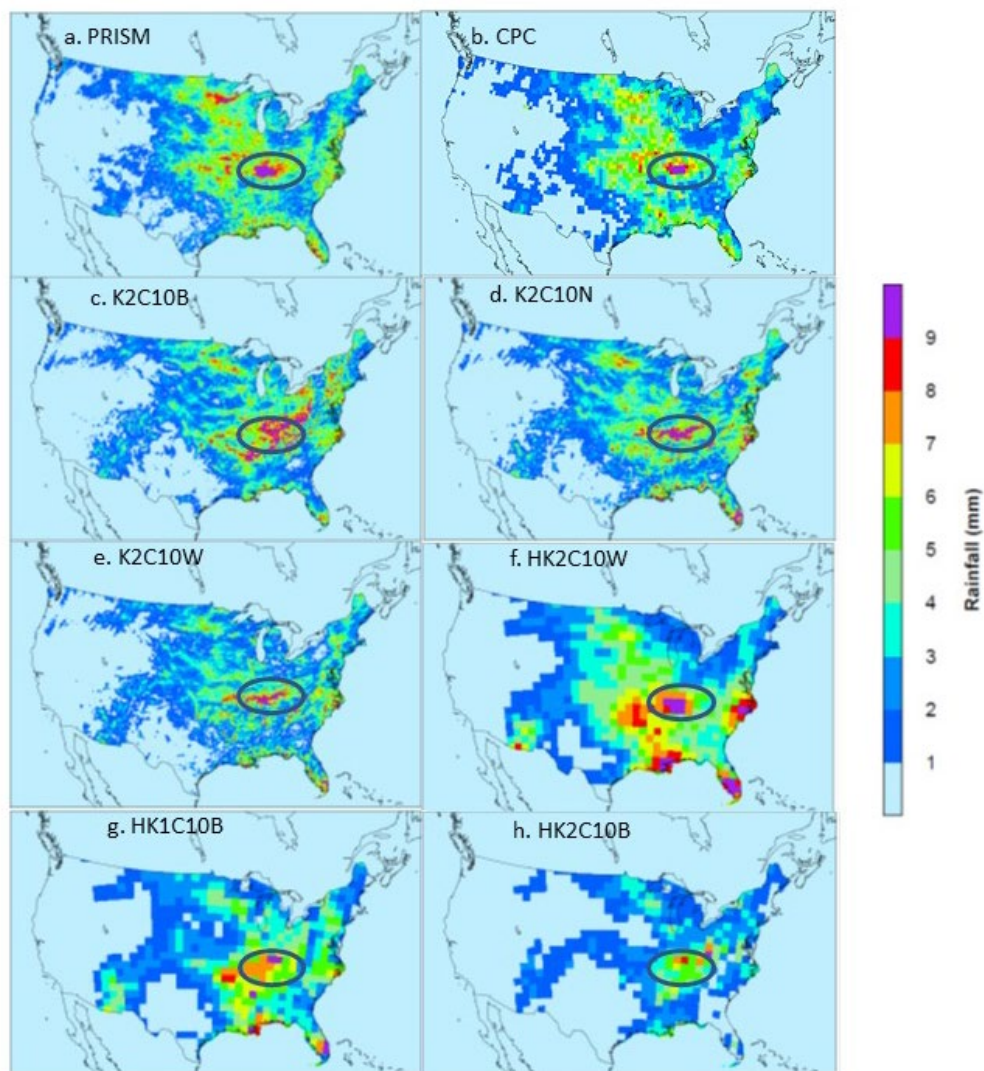
834

835 **Figure 10.** Same as Figure 8, but for RMSE.



836

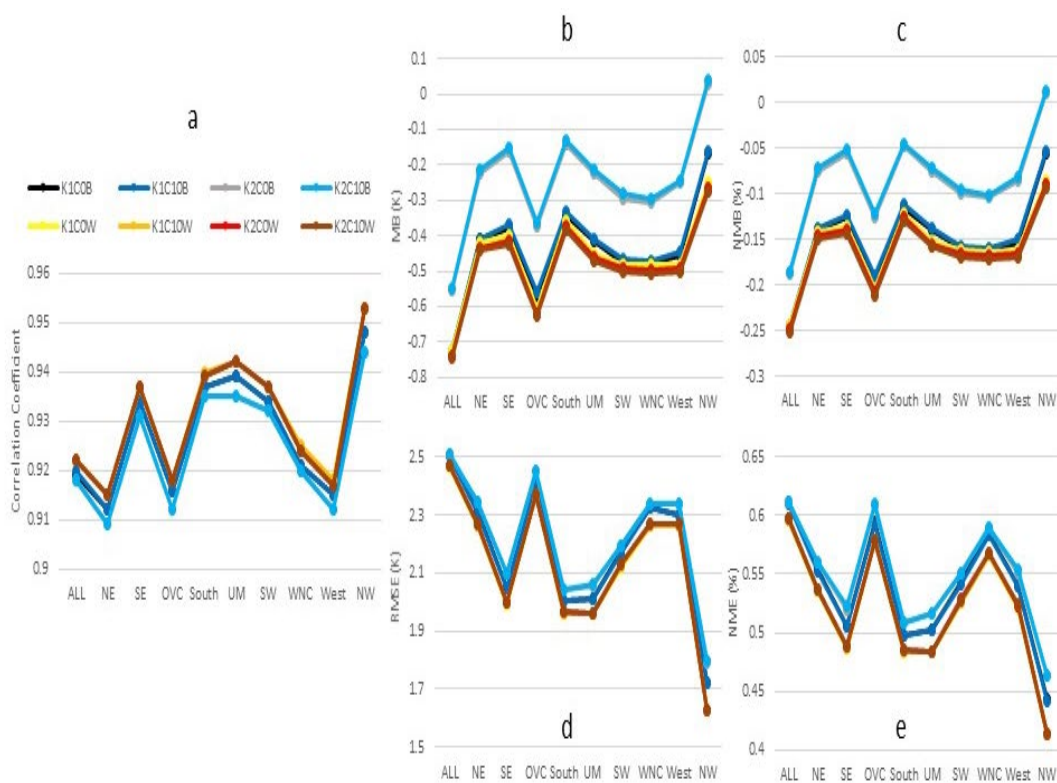
837 **Figure 11.** Same as Figure 8, but for MB.



838

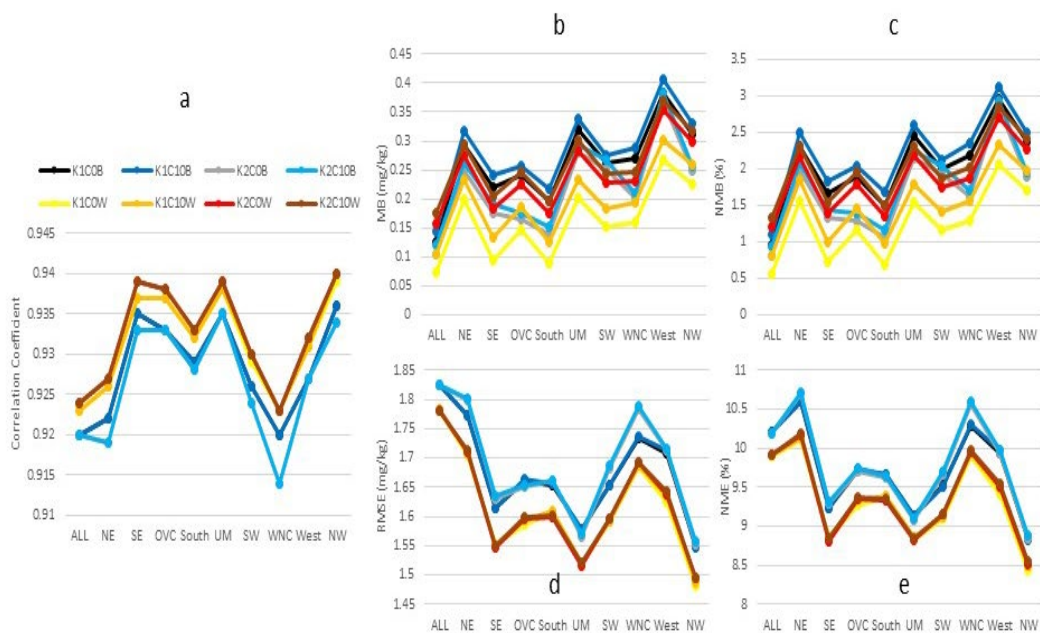
839 **Figure 12.** Mean daily precipitation over the CONUS during July 2016 from a) PRISM, b) CPC,  
840 c) K2C10B, d) K2C10N, e) K2C10W, and f) HK2C10W, g) HK1C10B, and h)  
841 HK2C10B. Note that all the observational based products and the 108 km hemispheric  
842 simulations are regridded onto the 12 km CONUS domain.

843



844

845 **Figure 13.** Monthly mean statistics for 2-m temperature from hemispheric BASE and LTA  
 846 simulations comparing to surface observations during July 2016: a) correlation coefficient, b)  
 847 MB, c) NMB, d) RMSE, and e) NME.



848

849 **Figure 14.** Same as Figure 12, but for 2-m water vapor mixing ratio.

850